

APPLICATION
FOR
UNITED STATES LETTERS PATENT

TITLE: NON-SPHERICAL WHISPERING-GALLERY-MODE
MICROCAVITY

APPLICANT: LUTFOLLAH MALEKI , XIAOTIAN S. YAO, AND
VLADIMIR ILCHENKO

CERTIFICATE OF MAILING BY EXPRESS MAIL

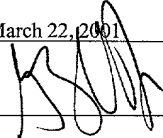
Express Mail Label No. EL 584 941 185

I hereby certify under 37 CFR §1.10 that this correspondence is being deposited with the United States Postal Service as Express Mail Post Office to Addressee with sufficient postage on the date indicated below and is addressed to the Commissioner for Patents, Washington, D.C. 20231.

Date of Deposit

March 22, 2001

Signature



Gildardo Vargas
Typed or Printed Name of Person Signing Certificate

NON-SPHERICAL WHISPERING-GALLERY-MODE MICROCAVITY

This application claims the benefit of U.S. Provisional Application No. 60/191,141, filed on March 22, 2000.

Origin

5 The systems and techniques described herein were made in the performance of work under a NASA contract, and are subject to the provisions of Public Law 96-517 (35 USC 202) in which the Contractor has elected to retain title.

Background

10 This application relates to optical resonators, and more specifically, to optical whispering-gallery-mode resonators.

A dielectric sphere may be used to form an optical whispering-gallery-mode resonator which supports a special set of resonator modes known as "whispering gallery modes". These 15 modes represent optical fields confined in an interior region close to the surface of the sphere around its equator due to the total internal reflection at the sphere boundary.

Microspheres with diameters on the order of $10\text{--}10^2$ microns have been used to form compact optical resonators. Such 20 resonators have a resonator dimension much larger than the wavelength of light so that the optical loss due to the finite curvature of the resonators can be small. The primary sources for optical loss include optical absorption in the dielectric

material and optical scattering due to the inhomogeneity of the sphere (e.g., irregularities on the sphere surface). As a result, a high quality factor, Q , may be achieved in such resonators. Some microspheres with sub-millimeter dimensions

5 have been demonstrated to exhibit very high quality factors for light waves, exceeding 10^9 for quartz microspheres.

Hence, optical energy, once coupled into a whispering gallery mode, can circulate at or near the sphere equator with a long photon life time.

10 Whispering-gallery-mode resonators may use resonator geometries based on spheres. Since the whispering gallery modes essentially exist near the equator of a sphere, a resonator may not be necessarily a whole sphere but a portion of the sphere near the equator that is sufficiently large to

15 support the whispering gallery modes. Hence, rings, disks and other geometries formed from a proper section of a sphere may be used. Such resonators are still spherical and their whispering gallery modes are essentially identical to such modes of the respective whole spheres.

20

Summary

This application includes non-spherical whispering-gallery-mode resonators and their applications. In one embodiment, a spheroidal cavity is used to generate a true

finesse on the order of 10^4 , a free spectral range of the order of few nanometers, and a quality-factor $Q \sim 1 \times 10^7$. Devices based on such a spheroidal cavity are also disclosed.

Brief Description of the Drawings

5 FIG. 1 shows one embodiment of a non-spherical microcavity.

FIGS. 2A, 2B, and 2C show exemplary evanescent coupling configurations for the non-spherical microcavity in FIG. 1.

10 FIG. 3 shows a photograph of a spheroidal cavity by compressing a small sphere of low-melting silica glass between cleaved fiber tips based on the design in FIG. 1 with $D = 2a = 165 \mu\text{m}$; $d = 42 \mu\text{m}$; and $2b = 83 \mu\text{m}$.

15 FIG. 4 shows the measured TE WG mode spectrum of the cavity shown in FIG. 2 by using a tunable DFB laser near the wavelength of 1550 nm Free spectral range.

FIGS. 5A, 5B, and 5C show embodiments of opto-electronic oscillators using a spheroidal cavity as an optical delay element in a feedback loop.

20 FIGS. 6A and 6B show two stabilized lasers based on frequency locking using a spheroidal cavity.

Detailed Description

The spheroidal microcavity geometry is designed in part based on recognition of fundamental characteristics and certain limitations of spherical microcavities formed from 5 partial or whole spheres. The whispering-gallery modes are essentially closed circular waves trapped by total internal reflection inside an axially symmetric dielectric body. The very high quality factors Q of microspheres may be attributed to several factors. For example, dielectric materials for 10 microspheres are selected to have ultra-low optical loss in at the frequencies of the supported whispering gallery modes. Fiber-grade fused silica may be used for resonators operating at wavelengths near 1.3 and 1.5 microns at which the optical loss is low. For another example, the surface of the sphere 15 may be specially fabricated to minimize the size of any surface inhomogeneities, e.g., on the order of a few Angstroms by processes such as fire polishing. The high index contrast in microsphere cavities is also used for steep reduction of radiative and scattering losses with increasing radius. In 20 addition, the two-dimensional curvature of a sphere provides for grazing reflection of all wave vector components. The grazing incidence in a sphere can be essential for minimizing surface scattering that would otherwise limit the Q far below that imposed by attenuation in the material. For example, in

the integrated optical micro-ring and micro-disk cavities based on planar waveguide technology, the light effectively bounces from flat surfaces under *finite* angles and their typical Q-factor is limited to $10^4 \sim 10^5$.

5 The substantially higher Q in spheres, as compared to micro-disks and micro-rings, comes at the price of a relatively dense spectrum of modes. In an ideal sphere with zero eccentricity, the optical spectrum of the sphere has $TE(TM)_{lmq}$ modes separated by a free spectral range (FSR) 10 defined by the circumference of the sphere and related to consecutive values of the mode index l . The mode index l approximately represent the number of wavelengths that fit into the optical length of the equator, m the number of field maxima in the equator plane, and q the field maxima in the 15 direction along the radius in the equator plane.

Each of $TE(TM)_{lmq}$ modes, however, is degenerate and includes $(2l+1)$ modes given by the possible values of the mode index m . In actual spheres, the spherical surfaces are usually not perfectly spherical and have residual 20 nonsphericity. This deviation from the perfect spherical surface lifts the mode degeneracy and breaks down each $TE(TM)_{lmq}$ mode with a given value for the mode index l into a series of observable $TE(TM)_{lmq}$ modes with different values in the mode index m under each value for the mode index l .

Therefore, a nonideal spherical resonator exhibits two different FSRs, a "large" FSR which is the frequency spacing between two adjacent $TE(TM)_{lmq}$ modes with the same values for indices m and q but with a difference of 1 in their l values,
5 and a "small" FSR which is the frequency spacing between two adjacent $TE(TM)_{lmq}$ modes with the same l values but with a difference of 1 in their m values:
difference of 1 in their m values:

"Small" FSR:

$$\nu_{lmq} - \nu_{l,m-1,q} \sim \nu \frac{\epsilon^2}{2l}$$

10 "Large" FSR:

$$\nu_{lmq} - \nu_{l-1,mq} = \frac{c}{2\pi n a} (t_{lq} - t_{l-1,q}) \sim \nu / l$$

In silica spheres of diameter 150 to 400 micron, for example, typical fabrication techniques usually produce an eccentricity of about $\epsilon^2 = 3 \times 10^{-2}$. The "large" FSR may be in
15 the range of 437 to 165GHz, or in the wavelength scale, 3.5 to 1.3nm near the center wavelength 1550nm. The "small" FSR may be in the range of 6.8 - 2.5GHz. As a result, the spheres are capable of producing a large FSR on the order of hundreds of GHz, the actual spectrum of such spheres are relatively dense
20 with a useful FSR limited by the "small" FSR typically under 10 GHz.

The above relatively dense spectrum in a typical sphere resonator may limit applications of the resonator since it can complicate spectral analysis, cause a mode hop caused by frequency jittering of a laser when such a resonator is used 5 as a frequency reference to lock a CW laser at a selected laser frequency. In addition, intermediate filtering may be needed to eliminate some of the modes to obtain a spectrum with well-separated resonance peaks.

Hence, one way to achieve a FSR on the order of hundreds 10 of GHz in spherical resonators without external spectral filtering is to maintain the mode degeneracy so that the "large" FSR in the whisper gallery modes $TE(TM)_{lmq}$ for given values in the mode index l can be produced in the resonator's spectrum. Under this approach, the eccentricity of the sphere 15 should be minimized. This, however, may be technically difficult due to practical limitations of the available fabrication technologies.

In recognition of the above, the microcavities in the present application are designed to use non-spherical 20 resonator geometries that are axially symmetric. Such a non-spherical resonator retains the two-dimensional curvature confinement, low scattering loss, and very high Q typical of microspheres, and yet approaches spectral properties of the single-mode waveguide ring. In one embodiment, instead of

minimizing the eccentricity, such a non-spherical resonator may be formed by distorting a sphere to a non-spherical geometry to purposely achieve a large eccentricity, e.g., greater than 10^{-1} . The following describes an oblate 5 spheroidal microcavity or microtorus as one example of such non-spherical microcavities.

FIG. 1 shows one embodiment of a spheroidal microcavity 100 formed of an optical dielectric material. The cavity 100 is formed by revolving an ellipse around a symmetric axis 10 along the short elliptical axis 101. The lengths of the long and short elliptical axes are a and b , respectively. Hence, the eccentricity of cavity 100 is $\epsilon^2 = (1-b^2/a^2)$. Near the 10 symmetry plane at the location of WG modes, toroidal surface of outer diameter D and cross-section diameter d coincides 15 with that of the osculating oblate spheroid with large semiaxis $a = D / 2$ and small semiaxis $b = \frac{1}{2}\sqrt{Dd}$. The dimension D of the spheroid 100 may be less than 10 mm for operations in the optical and microwave spectral ranges. The eccentricity may be greater than 0.5 for 20 In operation, at least one optical coupling element may be positioned near the cavity 100 to evanescently couple an input beam into the cavity 100 in one or more whispering gallery modes. An optical fiber or a planner waveguide

configured with an angle-polished facet may be used as this optical coupling element. A microprism may also be used to provide the proper evanescent coupling. FIGS. 2A and 2B show the above optical coupling mechanisms. FIG. 2C shows that, 5 when two such optical coupling elements are used, one is to couple light into the cavity 100 and the other is to couple light out of the cavity 100.

Analysis of the spectrum of the dielectric spheroid 100 is not a trivial task, even numerically. In contrast to a 10 sphere of a small eccentricity, analysis in highly-eccentric spheroids generally cannot be based on simple geometrical approximations. Unlike the case of cylindrical or spherical coordinates, orthogonal spheroidal vector harmonics that satisfy boundary conditions may not be derived via a single 15 scalar wave function. Furthermore, the calculation of spheroidal angular and radial functions is also a nontrivial task.

The WG mode eigenfrequencies of the cavity 100 for a radius a much larger than the wavelength of the a WD mode may 20 approximately represented as follows:

$$nk_{lmq}a \approx t_{lq} - \frac{\chi}{\sqrt{n^2 - 1}}, \quad (1)$$

where t_{lq} is the q -th zero of the spherical Bessel function of the order l and $\chi = n$ for TE -mode and $\chi = 1/n$ for TM -mode. For large l , $t_{lq} \sim l + O(l^{1/3})$, which may be calculated either directly or approximated via the zeroes of the Airy function.

5 See, e.g., M.Abramowitz, I.A.Stegun, eds., Handbook on mathematical functions, New-York, Dover Publ. (1970).

The meaning of small second term on the right hand side of Eq.(1) may be understood by considering the following.

First, a WG mode is quasiclassically a closed circular beam
10 supported by the total internal reflection within the cavity 100. Secondly, the optical field tunnels outside of the cavity 100 at the depth $1/k\sqrt{n^2-1}$. Thirdly, the tangential component of E (TE -mode) or the normal component of E (TM -mode) at the surface of the cavity 100 is continuous at the
15 boundary. Eigen frequencies of high-order WG modes ($l \gg 1; l \approx m$) in dielectric spheres can be approximated via solutions of the scalar wave equation with zero boundary conditions, because most of the energy is concentrated in one component of the field (E_θ for TE -mode and E_r for TM -mode).

20 Based on above considerations, the WG mode eigenfrequencies can be estimated for the oblate spheroid 100 of large semiaxis a , small semiaxis b , and eccentricity $\epsilon = \sqrt{1-b^2/a^2}$. Since WG modes are localized in the "equatorial"

plane, the radial distribution may be approximated by

cylindrical Bessel function $J_m(n\tilde{k}_{mq}r)$ with $n\tilde{k}_{mq}a = na\sqrt{k_{lmq}^2 - k_\perp^2} \approx T_{mq}$,

where $J_m(T_{mq})=0$ and k_\perp is the wavenumber for quasiclassical solution for angular spheroidal functions and can

5 approximately written as:

$$k_\perp^2 \approx \frac{2(l-m)+1}{a^2\sqrt{1-\varepsilon^2}}m.$$

more rigorous considerations can follow the approach given in

10 I.V.Komarov, L.I.Ponomarev, S.Yu.Slavyanov, Spheroidal and Coulomb Spheroidal Functions, Moscow, Nauka (1976). Taking into the account that $T_{mq} \approx t_{lq} - (l - m + 1/2)$, the following approximation can be derived:

$$15 nk_{lmq}a - \frac{\chi}{\sqrt{n^2-1}} \approx na\sqrt{\tilde{k}_{mq}^2 + k_\perp^2} \approx T_{mq} + \frac{k_\perp^2 a^2}{2T_{mq}} \approx t_{lq} + \frac{2(l-m)+1}{2} \left(\frac{1}{\sqrt{1-\varepsilon^2}} - 1 \right) \quad (2)$$

For very small ε , Eq.(2) yields the same value for "small" FSR (frequency splitting between modes with successive $m \approx l$).

See, e.g., H.M.Lai, P.T.Leung, K.Young, P.W.Barber, S.C.Hill,
20 Phys. Rev. A 41, 5187-5198 (1990).

The results of the approximation in Eq. (2) for $l = 100$ may be compared to numerically calculated zeroes of the radial spheroidal functions. Even with a large eccentricity of $\epsilon = 0.8$, the deviation is no more than 5% in the estimate of m ,
5 $m+1$ mode splitting and 0.1% in the absolute mode frequencies. For larger l and smaller ϵ , the error should evidently be smaller. As follows from Eq. (2), with increasing eccentricity ϵ , "small" FSR - frequency interval between modes with successive m - becomes compatible in magnitude with the

10 "large" FSR:

$$(k_{l+1mq} - k_{lmq}) \sim (k_{lm+1q} - k_{lmq}) \sim k_{lmq} / l .$$

In addition, excitation conditions for modes with different m
15 become more selective: e.g. optimal angles for prism coupling vary with ϵ as $\frac{k_{\perp}}{k_{lmq}} \propto (1 - \epsilon^2)^{-1/4}$.

FIG. 3 shows a photograph of a spheroidal (microtorus) cavity formed by compressing a small sphere of low-melting silica glass between cleaved fiber tips. The combined action
20 of surface tension and axial compression resulted in the desired spheroidal geometry. One of the fiber stems is then cut and the whole structure is installed next to a prism

coupler for evanescent coupling as shown in FIG. 2B for measurements.

FIG. 4 shows the measured WG mode spectrum by using a tunable DFB laser near the wavelength of 1550 nm. The laser 5 was continuously frequency-scannable within the range of ~80GHz by modulating the current, and from 1545.1 to 1552.4 nm by changing the laser temperature. The spectrum with a spectral range of 900 GHz was compiled from 15 individual scans with 60GHz increments obtained by changing the 10 temperature. The frequency reference for "stitching" the spectral fragments was obtained by recording the fringes of a high-finesse ($F \sim 120$) Fabry-Perot ethalon (FSR = 30 GHz) and additional frequency marks provided by 3.75 GHz amplitude modulation. The total drift of the FP was less than 400 MHz 15 over the full 15-minute measurement time. The spectrum is reduced to only two whispering-gallery modes of selected polarization excited within the "large" free spectral range of the cavity FSR = 383 GHz, or 3.06 nm in the wavelength domain. The transmission of "parasitic" modes is at least 6dB smaller 20 than that of the principal ones. With individual mode bandwidth of 23MHz, the finesse $F = 1.7 \times 10^4$ and $Q = 8.5 \times 10^6$ are therefore demonstrated with this micro-resonator.

The above measured result is comparable to the predictions of the approximate expression in Eq. (2). For a

$a = 82.5\mu\text{m}$, $b = 42.5\mu\text{m}$, the eccentricity is $\varepsilon = 0.86$. The refraction index of the dielectric material is $n = 1.453$. The principal mode number for TE -modes at the wavelength 1550nm should be $l \approx 473$. The "large" FSR is

5

$$\nu_{lmq} - \nu_{l-1,mq} = \frac{c}{2\pi n a} (t_{lq} - t_{l-1,q}) = \frac{c}{2\pi n a} (1 + 0.617l^{-2/3} + O(l^{-5/3})) \approx 402\text{GHz},$$

and the "small" FSR is

$$10 \quad \nu_{lmq} - \nu_{l,m-1,q} = \frac{c}{2\pi n a} \left(\frac{1}{\sqrt{1-\varepsilon^2}} - 1 \right) \approx 382\text{GHz}.$$

In the measured spectrum, the frequency separation between the largest peaks 1 and 2 in FIG. 4 is equal to 383.7 ± 0.5 GHz.

It may therefore be attributed as corresponding to the small

15 FSR, in good agreement with the above estimate, if we take

into account an approximately 2% uncertainty in the

measurement (limited mainly by the precision of geometrical evaluation of cavity dimensions). The separation between the

peaks 3 and 4 in Fig. 4, is equal to 400.3 ± 0.5 GHz, which

20 is close to the estimate value of the "large" free spectral range.

It may be argued that despite the large splitting between the modes with adjacent values of index m (of the order of "large" FSR), one may still expect a dense spectrum resulting from the overlap of many mode families with different 5 principal number l . In practice, however, it is exactly the coincidence in the frequency domain of WG modes with different main index l , and rapidly increasing difference $l - m$, that should be responsible for effective dephasing of the "idle" modes from the evanescent coupler, resulting in the reduction 10 of modes in the observed spectrum. In addition to increasing phase mismatch for excitation of WG modes with complex "transverse" structure ($l - m > 1$), reduced amplitude of these modes may also be the result of their lower intrinsic quality-factor. With smaller unloaded Q , critical coupling for these 15 modes would require closer position of the cavity to the excitation prism of waveguide.

The above examples and analysis indicate that a spheroidal microcavity can be designed to achieve a substantial reduction (up to 2 orders of magnitude) in the 20 number of excited WG modes in highly oblate spheroids compared to typical microspheres. This reduction in the mode density can be obtained without sacrificing the high Q associated with these structures. The novel type of optical microcavity demonstrates a true finesse on the order of 10^4 , a free

spectral range of the order of few nanometers, and a quality-factor $Q \sim 1 \times 10^7$. It is contemplated that a complete elimination of "transverse" WG modes may be expected in spheroidal cavities of higher eccentricity. Further increase 5 of the Q and the finesse may also be expected with a refinement of the fabrication technique. The decrease in the density of mode spectrum of ultra-high- Q microcavities offers new applications in laser stabilization, microlasers, various passive photonics devices, and in fundamental physics 10 experiments.

FIGS. 5A, 5B, and 5C show exemplary opto-electronic oscillators that use a spheroidal microcavity as an optical delay element. Compared to previously disclosed opto-electronic oscillators with microspheres operating in the 15 microwave band (typical frequencies ~ 3 - 30 GHz), the OEO based on micro-spheroidal (microtorus) resonator may operate robustly at much higher frequencies, corresponding to their mode spacing (FSR, free spectral range) in the submillimeter wave band (>300 GHz) and further, in Terahertz frequency 20 domain (>1000 GHz). Such an OEO may include an electrically controllable optical modulator 532 and at least one active opto-electronic feedback loop that comprises an optical part and an electrical part interconnected by a photodetector.

Although many commercial electro-optical modulators cannot

operate beyond 100GHz, such an ultra-high frequency optical modulator may be constructed on the basis of spheroidal resonator formed of electro-optic material as described later in this application. Modulator for the OEO needs not be
5 operated in wide range of frequencies, therefore high efficiency can be achieved by using double microwave and optical resonance. The opto-electronic feedback loop receives the modulated optical output from the modulator 532 and converted it into an electrical signal 524 to control the
10 modulator 532. The loop produces a desired delay and feeds the electrical signal in phase to the modulator 532 to generate and sustain both optical modulation and electrical oscillation in the RF range when the total loop gain of the active opto-electronic loop and any other additional feedback
15 loops exceeds the total loss.

The OEOs implement a CW signal laser 530 to produce a signal beam at an optical carrier frequency which may be tunable. The signal optical modulator 532 modulates the signal beam to produce the signal 536. The signal optical modulator 532 may be an amplitude modulator or a phase modulator. The phase modulator may be preferred in some applications because it is relatively simple to operate and can be designed to have low optical loss and operate without bias.

OEOs use optical modulation to produce oscillations in frequency spectral ranges that are outside the optical spectrum, such as in RF and microwave frequencies. The generated oscillating signals are tunable in frequencies and

5 can have narrow spectral linewidths and low phase noise in comparison with the signals produced by other RF and microwaves oscillators. Some examples of OEOs are disclosed in U.S. Patent Nos. 5,723,856, 5,777,778, 5,917,179, and 5,929,430, and U.S. Patent Application No. 09/491,988 filed

10 January 2000.

FIG. 5A shows a dual-loop OEO 500A in which an optical delay element 501 or 502 such as a fiber loop or the above optical spheroidal resonator is included in each opto-electronic feedback loop 510 or 520. Alternatively, one of

15 the feedback loops may be replaced with an electrical feedback loop. A RF coupler may be used to split a portion of the RF feedback signal 524 to produce an output RF signal 526. One feedback loop may be removed to form a single-loop OEO.

FIG. 5B shows a coupled OEO which directly couples a

20 laser oscillation in an optical feedback loop 530 to an electrical oscillation in an opto-electronic feedback loop 540 which includes an optical portion with an optical delay element 542 and an electrical portion that includes an optical-to-electrical conversion block 544 (e.g., a

photodetector). The optical gain of the optical feedback loop 530 is controllable by an electrical signal 524 from the opto-electronic loop 540, e.g., a semiconductor optical amplifier (SOA) 532 may be disposed in the optical loop 530. Here, the 5 optical feedback loop 530 and the SOA 532 function as the signal laser and the signal modulator 532 in FIG. 5A. A RF coupler 548 may be used to split a portion of the signal 524 as the output RF signal 526.

In addition, opto-electronic oscillators can also be 10 implemented by having at least one active opto-electronic feedback loop that generates an electrical modulation signal based on the stimulated Brillouin scattering. FIG. 5C shows such a Brillouin OEO which includes a Brillouin optical medium 560 in an opto-electronic feedback loop 562 and uses the 15 natural narrow linewidth of the Brillouin scattering to select a single oscillating mode. A pump laser 564 is used to generate a Brillouin pump beam in the Brillouin medium 560. A photodetector 566 converts the optical signal in the loop 562 into an electrical feedback signal equivalent to the RF signal 20 108. A RF coupler 548 may be used to split a portion of the detector output as the output RF signal 526.

The above spheroidal resonator operates to store optical energy only in certain whispering gallery modes. When the optical feedback caused by a round trip around the cavity has

a phase delay of $N2\pi$ ($N=1, 2, 3, \dots$), the optical resonator operates in a resonance and optical energy accumulates inside the resonator with a minimum loss. When the optical energy is coupled out at this resonance condition, the output is 5 maximized. However, when the optical feedback has a phase delay other than $N2\pi$, the amount of optical energy accumulated in the resonator reduces from its maximum value and, accordingly, the coupled output is also reduced from its maximum value. Thus, the resonator can be modulated to 10 produce a modulation on the output. The modulation on the phase delay is not limited to the phase difference between a resonance condition and a non-resonance condition and can be between any two different values in the phase delay. In fact, the phase delay may be biased at a value where a change in the 15 phase delay produces the maximum change in the output energy.

The dielectric material in the spheroidal resonator may be formed of an electro-optic material so that an external electrical signal can be used to change the refractive index of the resonator to change the whispering-gallery mode 20 condition and hence the output coupling. Such an optical modulator can be designed to operate at a low operating voltage on the millivolt level, to achieve a high modulation speed at hundreds of gigahertz or higher, and have a compact package. The optical coupling with the resonator may be

implemented with waveguides or fibers for integration with other fiber optical elements or integrated electro-optical circuits formed on substrates. Hence, such optical modulators may be used in a variety of applications having optical 5 modulation, including optical communication and optical signal processing.

Under proper configurations, either the spheroidal resonator alone or the spheroidal resonator in connection with a proper electrical strip line can form an electrical 10 resonator to support electrical energy in the same whispering gallery modes with proper phase matching conditions. Hence, electrical and optical waves can coexist and co-propagate in certain whispering gallery modes. When the sphere is formed of an electro-optic material, the electrical wave can be used 15 to alter or modulate the dielectric constant of the sphere and hence modulate the light based on the electro-optic effects.

It is further contemplated that, the spheroidal cavity may be formed of a laser-active material with action ions such as rare earth ions to operate as a miniature solid-state laser 20 when a proper optical pumping scheme is provided. The laser active material can produce an optical gain at a laser emission wavelength by absorbing pump light at a pump wavelength longer than the laser emission wavelength. Because of the small volume and high Q of whispering-gallery modes,

such a laser can combine very low threshold and narrow emission linewidth. For example, the angle-polished fiber coupler shown in FIG. 2A may be used to couple a pump beam into the spheroidal cavity and to couple the laser beam out of 5 the cavity, both through evanescent fields of the whispering gallery modes.

In particular, the pump beam need be coupled into a pump WG mode and the laser beam is generated within the cavity in a laser WG mode. Therefore, the angle of the end facet of the 10 fiber coupler is selected to match the mode matching conditions for both the pump and the laser beams. First, the fiber coupler matches the mode of the pump light guided by the fiber to a pump whispering gallery mode at the pump wavelength in the cavity. Secondly, the fiber coupler matches 15 at least one laser whispering gallery mode at the laser wavelength to a guided mode at the laser wavelength in the fiber so that the output laser beam can be transmitted in the fiber. Both the laser whispering gallery mode and the pump whispering gallery mode spatially overlap in the cavity 130 to 20 promote efficient energy conversion from the pump wavelength to the laser wavelength.

The above spheroidal (microtorus) resonators may also used to stabilize the frequency and narrow the emission linewidth of cw semiconductor diode lasers to take the

advantage of the well-separated and clean resonance peaks of the WD modes. FIGS. 6A and 6B show two examples. Because of very high Q of modes ($\sim 10^8$ instead of $\sim 10^2$ in diode laser cavity itself), frequency fluctuations in such a coupled 5 system can be suppressed by many order of magnitudes allowing creation of an ultracompact laser source with sub-kHz linewidth. This linewidth was previously achievable in larger-size cavity solid state lasers or complex stabilized systems based on external Fabry-Perot resonators.

10 This spherical microcavity was previously used in a system to stabilize a diode laser in an extra-cavity configuration. VASSILIEV VV, VELICHANSKY VL, ILCHENKO VS, GORODETSKY ML, HOLLBERG L, YAROVISTKY AV, Narrow-line-width diode laser with a high-Q microsphere resonator, OPT COMMUN 15 158: (1-6) 305-312 DEC 15 1998. That system, however, suffered from the excessive density of WG modes many of which (~100) were inside the gain bandwidth of laser diode (~several 15 nanometers) so that intermediate mode selectors had to be used to suppress instabilities. With spheroidal microcavities 20 configured to have their FSR in few nanometer domain, very simple configurations can be used as only one WG mode will find itself in the gain maximum of the semiconductor laser.

FIG. 6A depicts the embodiment of stabilized laser based on optical feedback provided by intracavity backscattering

effect. The output of the laser 610 is evanescently coupled into the cavity 100 as a wave 612 in a WG mode. The scattering of the wave 612 produces a counter-propagating wave 614 in a WG mode. The wave 614 is then coupled to control the 5 frequency of the laser 610. In FIG. 6B, a laser is formed by a closed optical that includes a semiconductor optical amplifier chip 620 (in effect, a laser diode with its internal cavity totally suppressed by antireflection coating), two passive waveguide or fiber couplers 630 and 640, and a 10 microspheroidal cavity 100. The frequency of the laser is locked at a WG mode of the cavity 100.

Although the present disclosure only includes a few embodiments, it is understood that various modifications and enhancements may be made without departing from the following 15 claims.